AWES2020
20th Australasian Wind Engineering Society Workshop
8 – 9 April, 2021

Transient aerodynamic characteristics of a square prism during an accelerating wind starting from quiescence

Ting Yang[1], Matthew Mason[2]
[1]The University of Queensland, t.yang@uq.edu.au.
[2]The University of Queensland, matthew.mason@uq.edu.au.

ABSTRACT

Wind loads on a square prism at a range of incidence angles $0° \leq \alpha \leq 45°$ subject to an accelerating wind starting from quiescence is experimentally investigated. This type of accelerating wind is generated by programming the wind tunnel fan in the University of Queensland to increase its rotational speed from zero to its maximum capacity over a predefined time period. For $\alpha = 0°$, examination of the time evolution of ensemble-averaged mean drag coefficients and fluctuating lift coefficients indicates a process of wake formation and development during the accelerating wind. It is hypothesized that the wake behind the square prism undergoes formation and elongation of two symmetrical vortices, until a critical Reynolds number, beyond which the wake loses its symmetry and starts to oscillate, which is around $\mathrm{Re} = 7.1{\sim}8.2 \times 10^3$. This far exceeds where this occurs in steady, smooth flow cases, i.e. $\mathrm{Re} \lesssim 46$. After the critical Reynolds number, the magnitude of mean drag coefficient and fluctuating lift coefficient develops over time and reaches a steady-state before the flow acceleration ends (for the flow conditions tested). Results at other incidence angles highlight an overshoot in the time history of ensemble-averaged mean drag coefficients and fluctuating lift coefficients for $12.5° \leq \alpha \leq 40°$, in excess of what is observed in steady flow tests. This is hypothesized to be due to the overaccumulated vorticity in the wake formation and development process in excess of the one in the final regularly vortex shedding wake, wherein part of vorticity fed by separating shear layers is locked into separation bubble formed on the side face. The case of $\alpha = 12.5°$ gives rise to the most pronounced response in the above two parameters, with the overshoot coefficient being 1.31 and 2.08, respectively.

1. Introduction

The flow around an impulsively started circular cylinder is one of the classic problems in regard to unsteady flow dynamics and has been investigated experimentally and numerically by a large number of researchers (e.g., Honji and Taneda, 1969, Nagata et al., 1975, Sarpkaya, 1978, and Bouard and Coutanceau, 1980). In addition, the cases of impulsively started square and other sharp-edged bluff cylinders have also been received considerable attention due to its practical importance in engineering applications (Sarpkaya and Ihrig, 1986, Tonui and Sumner, 2011, and Lorite-Díez et al., 2018). A common finding from the above literature is that the bluff body wake undergoes a process of vortex formation and development after the start of motion. Initially, a pair of symmetrical recirculation zone is formed behind the cylinder, which elongate with time. At a critical time, the wake becomes asymmetric, initiating the well-known Von Kármán vortex shedding.

This paper aims to investigate the transient aerodynamic characteristics of a fixed two-dimensional square prism subject to an accelerating wind starting from quiescence. This is analogous to the abovementioned cases wherein the object is moving through a stationary fluid. In addition, the effect of incidence angle on the resultant transient aerodynamic characteristics of the square prism is examined by rotating the model from $0°$ to $45°$.

2. Experimental setup

Experiments on the square prism at a range of incidence angles from 0° and 45° in steady and accelerating winds were conducted in an Eiffel-type open-loop wind tunnel at the University of Queensland. The tunnel has a test section that is 762mm wide, 762mm high and 2.38m long. The background flow turbulence level in the absence of model is measured to be less than 0.4%. The square prism model with a side length of 60mm is made from acrylic sheet. During experiments, it was horizontally suspended along the width of the test section and attached firmly to the mid-height of tunnel wall. To ensure two-dimensional flow conditions, one pair of circular end plates with diameter of 480mm were mounted symmetrically to either side of square prism with a distance of 600mm between them. The surface pressure measurements were performed simultaneously from pressure taps distributed over the mid-span circumference of square prism through the use of DPMS (TFI Corp.) at a sampling frequency of 1250Hz. There are 11 taps on windward and leeward faces and 12 taps on top and bottom faces. A cobra probe was placed 120mm off the ceiling of tunnel and aligned with the windward face of square prism, when it was placed normal to the wind, to measure the reference wind velocity. A tap located at the tunnel floor aligning with the position of cobra probe was used to measure the reference static pressure in the tunnel.

The steady wind is created by operating the axial fan to run at a constant rotational speed over a time duration of 180s. The accelerating wind is generated by programming the fan to increase from zero to a target value at its maximum possible rate. The target wind speed was maintained for at least 60s. For each incidence angle, accelerating wind tests were repeated 30 times to enable ensemble averaging analysis. The constant target wind speed was set to be approximately 12.0m/s for each incidence angle case with a variation of $\pm 2\%$. The resultant ensemble wind speed time histories for all incidence angle tests are shown in Figure 1. Plots are shown in terms of dimensionless $\langle U \rangle / U_t$ wherein $\langle U \rangle$ refers to the ensemble-averaged wind velocity calculated from the 30-repeat U measurements and U_t is the target wind speed, taken as the average of 25-s $\langle U \rangle$ data following the period of acceleration.

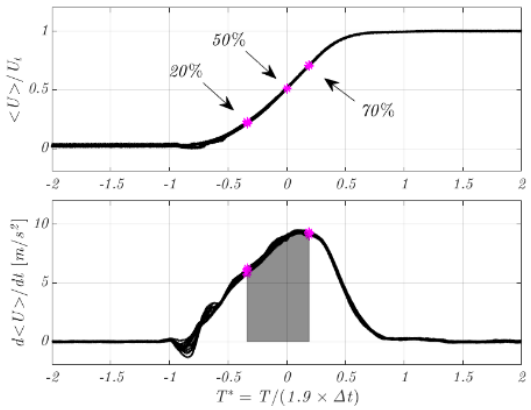

Figure 1 Time history of (a) ensemble-averaged velocity $\langle U \rangle$ normalized by its respective target velocity U_t, and (b) rate of change of ensemble-averaged velocity, $d\langle U \rangle/dt$ for all test cases.

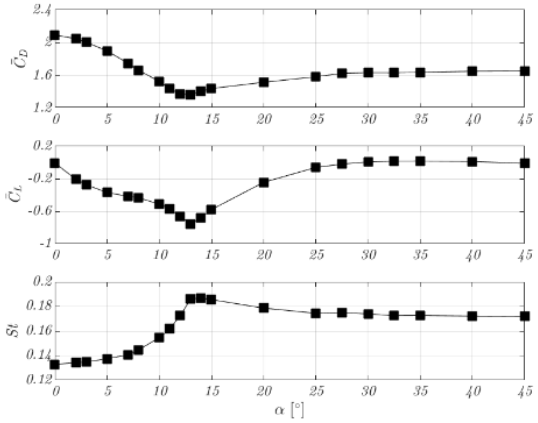

Figure 2 Variation of (a) $\bar{C}_D$, (b) $\bar{C}_L$ and (c) St of square prism with respect to incidence angles at $\mathrm{Re} = 3.2 \times 10^4$

Furthermore, the rate of change of $\langle U \rangle$, $d\langle U \rangle/dt$ at each instant in time is obtained by taking the localized slope of $\langle U \rangle - T$ within a 0.1-s window backward of that time point. Time is normalized by $T^* = T/(1.9 \times \Delta t)$ to make the start of flow acceleration occur at approximately $T^* = -1$, wherein Δt is the time gap between the first exceedance of 20% and 70% of the difference between the start and target wind speed. Note also that $T^* = 0$ is linked with the first exceedance of 50% of the start-target

wind speed difference. From the two plots in Figure 1, both the velocity and acceleration time histories are shown to collapse for all incidence angle cases. The shaded area under the curve of $d\langle U\rangle/dt$ bounded by the 20% and 70% velocity points is added up to determine the acceleration, a, used here to describe the flow. A dimensionless acceleration parameter is defined herein by $a_p = aD/(\frac{1}{2}(U_s + U_t))^2$ for direct comparison with other experimental results from the authors and available experimental results from previous literature. The a and equivalent a_p obtained here are 8.1~8.3m/s^2 and 0.013 for all incidence angle cases.

3. Effect of incidence angle in steady wind tests

The results obtained for a square prism at incidence in steady winds are presented in Figure 2. The pressure measurements were made at $\mathrm{Re} = 3.2 \times 10^4$ and the incidence angle was varied from $\alpha = 0°$ to $45°$. The surface pressures in the along-wind direction were integrated to yield drag force F_D and drag coefficient $C_D = F_D/(0.5\rho\overline{U}^2D')$, wherein ρ is the air density, $\overline{U}$ the time-averaged wind velocity and D' the projected cylinder depth in the cross-wind direction. Likewise, the surface pressures in the cross-wind direction were integrated to yield lift force F_L and lift coefficient $C_L = F_L/(0.5\rho\overline{U}^2B')$, wherein B' is the projected cylinder width in the along-wind direction. Figure 2 shows the variation of time-averaged drag and lift coefficient, $\bar{C}_D$ and $\bar{C}_L$, together with Strouhal number, i.e., dimensionless vortex shedding frequency which is estimated from the dominant frequency associated with the spectral peak of the fluctuating lift coefficient time history.

Overall, there is an abrupt change occurring in the curves of $\overline{C}_D$, $\overline{C}_L$ and St versus α at more or less the same critical incidence angle. This is believed to be due to the onset of reattachment of separated shear layer onto the lower side face of the model, which is confirmed by the flow visualization measurements of Huang et al. (2010), and Sohankar et al. (2015). $\bar{C}_D$ reaches its minimum value of 1.37 at $\alpha = 13°$, $\bar{C}_L$ reaches its minimum value of -0.79 at $\alpha = 13°$, and St reaches it maximum value of 0.187 at $\alpha = 14°$. These results agree well with those reported by the previous literature including Norberg (1993), Luo et al. (1994), and Huang and Lin (2011).

Therefore, the investigation of the effect of incidence angle on the aerodynamic characteristics of square prism highlights the occurrence of separation bubble on the lower side face (i.e., an enclosed area formed by reattaching shear layer and solid boundary) starting from the critical incidence angle of around $13°$. Beyond this incidence angle, the separation bubble is hypothesized to shrink in size progressively with a further increase in incidence angle. When α is in the range of $30°$ to $45°$, the separation bubble diminishes to a negligible level and has little influence on the resultant aerodynamic responses, e.g. $\overline{C}_D$, $\overline{C}_L$ and St of square prism.

4. The delayed onset of wake instability as a result of wind acceleration

Instantaneous drag and lift coefficient are calculated based on $C_{D,t} = \frac{F_{D,t}}{\frac{1}{2}\rho U(t)^2 D'}$ and $C_{L,t} = \frac{F_{L,t}}{\frac{1}{2}\rho U(t)^2 B'}$ and plotted in Figure 3(a) and (b). In the above expressions, $F_{D,t}$ and $F_{L,t}$ are drag and lift forces integrated from surface pressures in the along-wind and cross-wind directions, respectively, $U(t)$ is the instantaneous wind velocity measured by the cobra probe. At each time instant, a moving window of length $1/4T_t$ (i.e., T_t is the average shedding cycle period at the constant target wind velocity stage) is applied to calculate the ensemble-averaged mean and peak drag and lift coefficient. To be more specific, $\langle C_D\rangle$ and $\langle C_L\rangle$ are the mean value of the 30-repeat $C_{D,t}$ and $C_{L,t}$ data within that localized time window. $\langle \hat{C}_D\rangle$, $\langle \check{C}_D\rangle$, $\langle \hat{C}_L\rangle$ and $\langle \check{C}_L\rangle$ are the 95th and 5th percentile bounds of the same $C_{D,t}$ and $C_{L,t}$ data block. In addition, a 0.1-s smoothing window is applied when plotting them here.

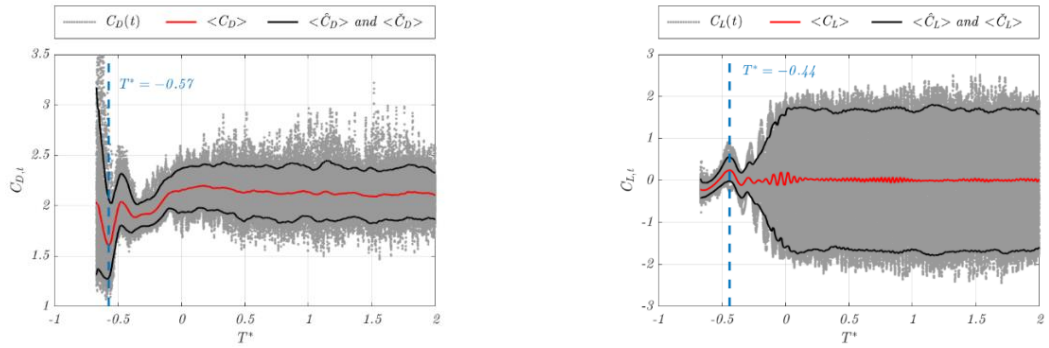

(a) $C_{D,t}$, $\alpha = 0°$ (b) $C_{L,t}$, $\alpha = 0°$

Figure 3 Time evolution of (a) $C_{D,t}$ and (b) $C_{L,t}$ in case of square prism at $\alpha = 0°$.

In Figure 3(a) and (b), the $C_{D,t}$ and $C_{L,t}$ data corresponding to wind velocity less than 0.8m/s are all removed because of the inaccuracy of cobra probe and DPMS instrument. The prominent feature of these two plots is the appearance of an inflection point in terms of time-dependent $\langle C_D \rangle$ and $\langle C_L \rangle$ after flow starts to accelerate. There is a slight discrepancy between the position of these two inflection points, with the one in $\langle C_D \rangle - T^*$ earlier than the one in $\langle C_L \rangle - T^*$. It is hypothesized that the first inflection point ($T^* = -0.44$) is indicative of the onset of wake instability after a stage of symmetrical vortex formation and elongation. The corresponding Reynolds number is 7.8×10^3, which is two orders of magnitude larger than in the steady flow cases, $\mathrm{Re} \lesssim 46$ reported by Jiang and Cheng (2018).

Results of $\langle C_L \rangle - T^*$ (Figure 4) and $\langle C_D \rangle - T^*$ (Figure 5) for the square prism through a range of incidence angle cases also reveals the same prominent features. The first inflection point of $\langle C_L \rangle - T^*$across all incidence angles cases is observed to occur at more or less the same Reynolds number (time instant), $\mathrm{Re} = 7.1 \sim 8.2 \times 10^3$. This indicates that the wake instability is intrinsically dependent on flow Reynolds number and in all cases, the flow acceleration delays the occurrence of wake instability. After the first inflection point in $\langle C_D \rangle$ and $\langle C_L \rangle$, both $\langle C_D \rangle$ and $\langle C_L \rangle$ starts to develop progressively with time, and reach their respective steady-state values at around $T^* = 0.5$, just after the peak value of flow acceleration (Figure 1). This indicates that the final vortex shedding regime is well-established before flow acceleration ends.

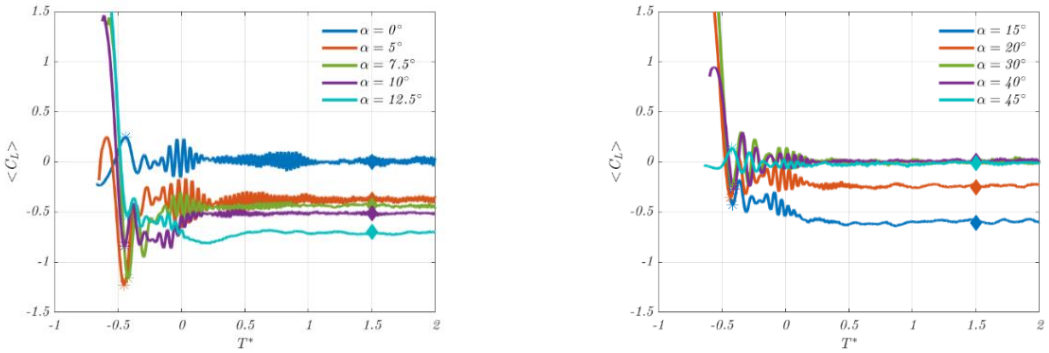

(a) $\langle C_L \rangle$, $0° \leq \alpha \leq 12.5°$ (b) $\langle C_L \rangle$, $15° \leq \alpha \leq 45°$

Figure 4 Time evolution of ensemble-averaged lift coefficient, $\langle C_L \rangle$, for (a) $0° \leq \alpha \leq 12.5°$ and (b) $15° \leq \alpha \leq 45°$. The diamonds mark the steady flow results.

5. Characterization of overshoot phenomenon

Another prominent feature of the transient aerodynamic characteristics of square prism at incidence in an accelerating wind starting from quiescence is the overshoot phenomenon appearing in curves of $\langle C_D \rangle$ and $(\langle \hat{C}_L \rangle - \langle \check{C}_L \rangle)/2$ versus T^* at $12.5° \leq \alpha \leq 40°$, as shown in Figure 5(a), (b), (c) and (d). This

refers to an unusually large value of $\langle C_D \rangle$ and $(\langle \hat{C}_L \rangle - \langle \check{C}_L \rangle)/2$ during the development of wake, which is in excess of the one in the final constant target wind velocity stage. This incidence angle range is corresponding to the separation bubble flow regime as discussed in Section 3. The overshoot phenomenon in $\langle C_D \rangle$ and $(\langle \hat{C}_L \rangle - \langle \check{C}_L \rangle)/2$ is hypothesized to be due to the overaccumulated vorticity behind the cylinder in the wake formation and development process, which is in excess of the one in the well-established vortex shedding regime, wherein part of the vorticity fed by the separated shear layer is locked into the separation bubble on the lower side face.

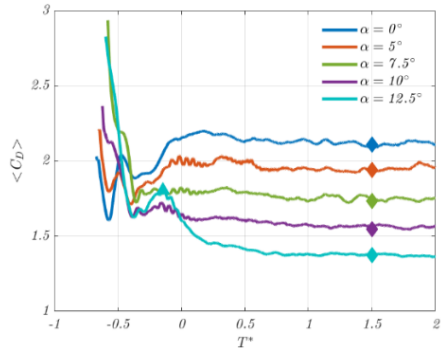

(a) $\langle C_D \rangle$, 0° ≤ α ≤ 12.5°

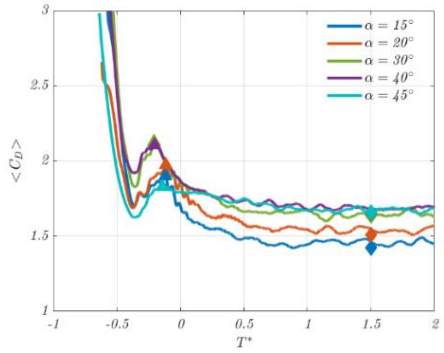

(b) $\langle C_D \rangle$, 15° ≤ α ≤ 45°

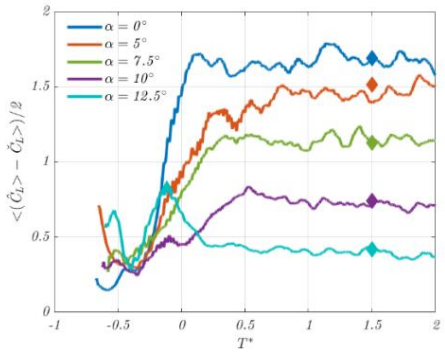

(c) $(\langle \hat{C}_L \rangle - \langle \check{C}_L \rangle)/2$, 0° ≤ α ≤ 12.5°

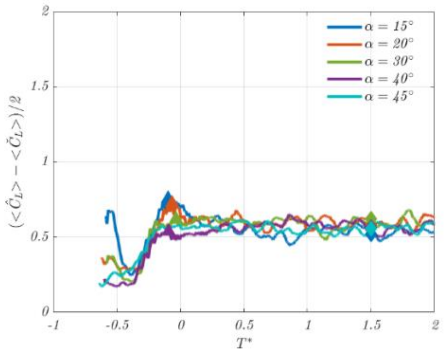

(d) $(\langle \hat{C}_L \rangle - \langle \check{C}_L \rangle)/2$, 15° ≤ α ≤ 45°

Figure 5 Time evolution of ensemble-averaged drag coefficient, $\langle C_D \rangle$ (a) 0° ≤ α ≤ 12.5° and (b) 15° ≤ α ≤ 45°and fluctuating lift coefficient, $(\langle \hat{C}_L \rangle - \langle \check{C}_L \rangle)/2$ for (c) 15° ≤ α ≤ 45° and (d) ° ≤ α ≤ 45°. Diamonds mark the steady flow results.

An overshoot coefficient is defined herein to evaluate the relative magnitude of the peak $\langle C_D \rangle$ and $(\langle \hat{C}_L \rangle - \langle \check{C}_L \rangle)/2$ as compared with the steady-state results (averaged over 3-s of data) in the final target wind velocity stage, denoted by $\Phi_{\langle C_D \rangle}$ and $\Phi_{(\langle \hat{C}_L \rangle - \langle \check{C}_L \rangle)/2}$ respectively. Table 1 lists the position and magnitude of the overshoot $\langle C_D \rangle$ and $(\langle \hat{C}_L \rangle - \langle \check{C}_L \rangle)/2$. It is evident that the case of $\alpha = 12.5°$ gives rise to the largest $\Phi_{\langle C_D \rangle}$ and $\Phi_{(\langle \hat{C}_L \rangle - \langle \check{C}_L \rangle)/2}$, with the value being 1.31 and 2.08 respectively. It is presumably due to the larger size of separation bubble formed on the lower side face, leading to the largest vorticity loss in the wake. With a further increase in α the $\Phi_{\langle C_D \rangle}$ shows little variation whereas the $\Phi_{(\langle \hat{C}_L \rangle - \langle \check{C}_L \rangle)/2}$ diminishes gradually until no overshoot arises at $\alpha = 40°$.

Table 1 Time and magnitude of the overshoot in $\langle C_D \rangle$ and $(\langle \hat{C}_L \rangle - \langle \check{C}_L \rangle)/2$

Incidence angles	$\langle C_D \rangle$		$(\langle \hat{C}_L \rangle - \langle \check{C}_L \rangle)/2$	
	T^*_{peak}	$\Phi_{\langle C_D \rangle}$	T^*_{peak}	$\Phi_{(\langle \hat{C}_L \rangle - \langle \check{C}_L \rangle)/2}$
$\alpha = 12.5°$	**-0.14**	**1.31**	**-0.11**	**2.08**
$\alpha = 15°$	-0.12	1.30	-0.10	1.42
$\alpha = 20°$	-0.11	1.28	-0.09	1.22
$\alpha = 30°$	-0.20	1.29	-0.06	1.05
$\alpha = 40°$	-0.20	1.25		

6. Conclusions

Three main findings from the above results and discussion are summarized as follows.

(1) The investigation of the effect of incidence angle on the aerodynamic characteristics of square prism in steady winds highlights the occurrence of separation bubble on the lower side face if the cylinder rotates in a clockwise direction (i.e., an enclosed area formed by reattaching shear layer and solid boundary) starting from the critical incidence angle of around $13°$.

(2) For the case of square prism subject to an accelerating wind starting from quiescence, the onset of wake instability is delayed by the presence of flow acceleration to a larger Reynolds number than in steady flow, $\mathrm{Re} = 7.1{\sim}8.2 \times 10^3$ across all incidence angles cases. This is two orders of magnitude larger than that of steady flow cases, $\mathrm{Re} \lesssim 46$. Before the onset of wake instability, the cylinder wake is hypothesized to be characterized by symmetric vortices which elongate with time. After the onset of wake instability, the mean drag coefficient and fluctuating lift coefficient develops with time, and reach their respective steady-state values before the period of acceleration ends. This indicates that the growth (break-up) of wake instability before the final establishment of vortex shedding regime.

(3) An overshoot phenomenon was found in the time evolution of both mean drag coefficient and fluctuating lift coefficient in the case of square prism at $12.5° \leq \alpha \leq 40°$. This was not the case for $\alpha < 12.5°$. This is hypothesized to be due to the overaccumulated vorticity during the vortex formation, elongation and growth of wake instability process, in excess of that in the final vortex shedding process, wherein part of the vorticity fed by separated shear layers is locked into the separation bubble formed on the side face. The case of $\alpha = 12.5°$ gives rise to the largest $\Phi_{\langle C_D \rangle}$ and $\Phi_{(\langle \hat{C}_L \rangle - \langle \check{C}_L \rangle)/2}$, with the value being 1.31 and 2.08 respectively, presumably due to the largest separation bubble formed on the lower side face, which causes the largest vorticity loss.

References

Bouard, R. and M. Coutanceau (1980). "The early stage of development of the wake behind an impulsively started cylinder for 40< Re< 104." Journal of Fluid Mechanics **101**(3): 583-607.

Honji, H. and S. Taneda (1969). "Unsteady flow past a circular cylinder." Journal of the physical society of Japan **27**(6): 1668-1677.

Huang, R. and B. Lin (2011). "Effects of flow patterns on aerodynamic forces of a square prism at incidence." Journal of Mechanics **27**(3): 347-355.

Huang, R., B. Lin and S. Yen (2010). "Time-averaged topological flow patterns and their influence on vortex shedding of a square prism in crossflow at incidence." Journal of Fluids and Structures **26**(3): 406-429.

Jiang, H. and L. J. P. o. F. Cheng (2018). "Hydrodynamic characteristics of flow past a square prism at moderate Reynolds numbers." **30**(10): 104107.

Lorite-Díez, M., J. Jiménez-González, C. Gutiérrez-Montes and C. Martínez-Bazán (2018). "Effects of rear cavities on the wake behind an accelerating D-shaped bluff body." Physics of Fluids **30**(4): 044103.

Luo, S., M. G. Yazdani, Y. Chew and T. Lee (1994). "Effects of incidence and afterbody shape on flow past bluff cylinders." Journal of wind engineering and industrial aerodynamics **53**(3): 375-399.

Nagata, H., Y. Kakehi, M. TSUNEKAWA and T. Hasegawa (1975). "Unsteady flow past a circular cylinder started impulsively." Bulletin of JSME **18**(123): 992-1001.

Norberg, C. (1993). "Flow around rectangular cylinders: pressure forces and wake frequencies." Journal of wind engineering and industrial aerodynamics **49**(1-3): 187-196.

Sarpkaya, T. (1978). Impulsive Flow about a Circular Cylinder, NAVAL POSTGRADUATE SCHOOL MONTEREY CALIF.

Sarpkaya, T. and C. Ihrig (1986). "Impulsively started steady flow about rectangular prisms: experiments and discrete vortex analysis." Journal of fluids engineering **108**(1): 47-54.

Sohankar, A., S. Mohagheghian, A. A. Dehghan and M. D. Manshadi (2015). "A smoke visualization study of the flow over a square prism at incidence and tandem square prisms." Journal of Visualization **18**(4): 687-703.

Tonui, N. and D. Sumner (2011). "Flow around impulsively started square prisms." Journal of fluids and structures **27**(1): 62-75.